

Phase-field simulation of electric-field-induced in-plane magnetic domain switching in magnetic/ferroelectric layered heterostructures

Jia-Mian Hu, G. Sheng, J. X. Zhang, C. W. Nan, and L. Q. Chen

Citation: *J. Appl. Phys.* **109**, 123917 (2011); doi: 10.1063/1.3600203

View online: <http://dx.doi.org/10.1063/1.3600203>

View Table of Contents: <http://jap.aip.org/resource/1/JAPIAU/v109/i12>

Published by the [American Institute of Physics](#).

Related Articles

Spin configurations in $\text{Co}_2\text{FeAl}_{0.4}\text{Si}_{0.6}$ Heusler alloy thin film elements
Appl. Phys. Lett. **99**, 182510 (2011)

Quantum tunneling of the Bloch point in a magnetic film with strong uniaxial magnetic anisotropy
Low Temp. Phys. **37**, 690 (2011)

Evolution of magnetic bubble domains in manganite films
Appl. Phys. Lett. **99**, 042503 (2011)

360° domain wall mediated reversal in rhombic Co/Cu/NiFe magnetic rings
Appl. Phys. Lett. **98**, 252506 (2011)

Transformations of head-to-head domain walls in $(\text{La,Sr})\text{MnO}_3$ thin films
J. Appl. Phys. **109**, 113901 (2011)

Additional information on J. Appl. Phys.

Journal Homepage: <http://jap.aip.org/>

Journal Information: http://jap.aip.org/about/about_the_journal

Top downloads: http://jap.aip.org/features/most_downloaded

Information for Authors: <http://jap.aip.org/authors>

ADVERTISEMENT

**AIP**Advances

Submit Now

**Explore AIP's new
open-access journal**

- **Article-level metrics
now available**
- **Join the conversation!
Rate & comment on articles**

Phase-field simulation of electric-field-induced in-plane magnetic domain switching in magnetic/ferroelectric layered heterostructures

Jia-Mian Hu,^{1,2,a)} G. Sheng,² J. X. Zhang,^{2,b)} C. W. Nan,¹ and L. Q. Chen²

¹Department of Materials Science and Engineering, and State Key Lab of New Ceramics and Fine Processing, Tsinghua University, Beijing 100084, China

²Department of Materials Science and Engineering, The Pennsylvania State University, University Park, 16802, USA

(Received 8 March 2011; accepted 12 May 2011; published online 22 June 2011)

The electric-field-induced in-plane magnetic domain switching in magnetic/ferroelectric (FE) layered heterostructures was studied using phase-field simulations. In particular, we chose the CoFe_2O_4 (CFO) magnetic film and the $\text{Pb}(\text{Zn}_{1/3}\text{Nb}_{2/3})\text{O}_3$ – PbTiO_3 (PZN-PT) FE layer as a representative example due to their strong respective magnetoelastic and piezoelectric couplings. In-plane 90° magnetic domain switching in the CFO film was observed when a transverse electric field was applied to the PZN-PT layer. The detailed switching behaviors as well as the corresponding magnetic domain structures are presented for CFO films with different geometric sizes and initial magnetization configurations. The effect of a *dynamic* electric field on the switching process, i.e., a time-dependent electric-field-induced magnetic domain switching, is also discussed. © 2011 American Institute of Physics. [doi:10.1063/1.3600203]

I. INTRODUCTION

Switching magnetic domain or magnetization directly via electric fields rather than current, i.e., the converse magnetoelectric (ME) effect,^{1,2} has drawn much attention in the fields of spintronics and multiferroics.^{3,4} It is a critically important step for realizing the applications of purely voltage-driven devices with much lower power consumption and higher speed.^{5,6} Such an electric-field-induced switching behavior has been reported in diluted magnetic semiconductors and oxides^{4,7} as well as ultra-thin ferromagnetic metal films.^{8,9} However, such effects observed in these materials are all limited to low temperature (far below room temperature) and/or high switching electric fields (1 MV cm^{-1} or higher).

An alternative approach to engineering low electric-field-induced magnetic domain switching at room temperature is to artificially design multiferroic heterostructures of magnetic and ferroelectric (FE) layers,^{1,10} which directly couple the magnetization and electric polarizations across the interface. The ME effect in such magnetic/ferroelectric heterostructures can be induced as a result of mechanical coupling,^{11–15} magnetic exchange bias,^{16–18} and interface-charge based couplings,^{19,20} depending on both the intrinsic material properties¹⁰ and the size effect.²¹ Among them, the strain-mediated ME coupling is understood as a product effect¹ based on the mechanical transfer between different phases of the heterostructures, which has received increasing interest since firstly reported in the early 1970s.²² While its physical origin is straightforward, the details remain elusive,¹⁰ especially for the converse ME coupling, i.e., the electric-field-controlled magnetic domain switching.

In our previous theoretical analysis² based on thermodynamic calculations, we demonstrated that the easy axis (i.e., spontaneous magnetization) of the magnetic thin film can be switched from an initial in-plane to an out-of-plane direction by applying a longitudinal electric field to the attached FE layer, while a transverse electric field can induce a 90° in-plane switching. Zhong *et al.* also investigated the electric field controlled magnetization in such multiferroic layered heterostructures using a similar phenomenological approach.²³ However, a single domain magnetic film was employed in both studies for simplicity, and the calculations are limited to *static* switching processes, i.e., the applied electric fields are uniform and independent of time.

To model the realistic multi-domain structure and *dynamic* time-dependent electric-field-induced magnetic domain switching process in these magnetic/ferroelectric layered heterostructures, the phase-field method is employed by considering the inhomogeneous spatial distributions of polarization and the magnetization fields.^{24–28} We reported the preliminary results on out-of-plane magnetic domain switching under isotropic biaxial strains in an earlier publication.²⁹ In this paper, we will focus on the electric-field-induced 90° in-plane switching, which, in principle, requires a lower critical switching electric field.² This feature could be potentially utilized to develop novel strain-mediated ME memories^{30,31} or logic devices.³² The rest of the paper will be organized as follows: After briefly introducing the model system and the phase-field approach in Sec. II, the electric-field-induced domain switching features and corresponding domain structures under various electric fields are discussed in Sec. III. The influences of different geometric sizes as well as initial magnetization configurations in the magnetic layers are considered. Domain switching behaviors under *dynamic* electric fields, i.e., a time-dependent electric-field-induced magnetic domain switching, are presented in Sec. IV. The conclusions are given in Sec. V.

^{a)}Author to whom correspondence should be addressed. Electronic mail: hjm08@mails.tsinghua.edu.cn.

^{b)}Current address: Research and Development, Carpenter Technology Corporation, Reading, PA 19601, USA.

II. MODEL

We consider a simple bilayered multiferroic heterostructure with a magnetic film directly grown on its attached ferroelectric (FE) layer, as shown in Fig. 1. A transverse electric field is applied to the FE layer to generate anisotropic in-plane piezostains, which can be mediated to the top magnetic layer and further induce an in-plane magnetic domain switching via magnetoelastic coupling.^{2,30}

In the phase-field approach, the magnetic domain structure is described by the spatial distribution of the local magnetization vectors $\mathbf{M} = M_s \mathbf{m} = M_s(m_1, m_2, m_3)$, where M_s and m_i ($i = 1, 2, 3$) represent the saturation magnetization and the direction cosine, respectively. The temporal evolution of the magnetization configuration and, thus, the domain structure is governed by the Landau-Lifshitz-Gilbert (LLG) equation, i.e.,

$$(1 + \alpha^2) \frac{\partial \mathbf{M}}{\partial t} = -\gamma_0 \mathbf{M} \times \mathbf{H}_{\text{eff}} - \frac{\gamma_0 \alpha}{M_s} \mathbf{M} \times (\mathbf{M} \times \mathbf{H}_{\text{eff}}), \quad (1)$$

where γ_0 and α are the gyromagnetic ratio and the damping constant, respectively, and \mathbf{H}_{eff} the effective magnetic field, given as $\mathbf{H}_{\text{eff}} = -(1/\mu_0 M_s)(\partial F_{\text{tot}}/\partial \mathbf{m})$. Here μ_0 denotes the vacuum permeability, and F_{tot} is the total free energy of a multi-domain magnetic film, expressed by

$$F_{\text{tot}} = F_{mc} + F_{ms} + F_{ex} + F_{elas}, \quad (2)$$

where F_{mc} , F_{ms} , F_{ex} , and F_{elas} are the magnetocrystalline anisotropy, magnetostatic, magnetic exchange, and elastic energy, respectively. Among them, the magnetocrystalline anisotropy energy of a cubic ferromagnet can be expressed as,

$$F_{mc} = \int [K_1(m_1^2 m_2^2 + m_1^2 m_3^2 + m_2^2 m_3^2) + K_2 m_1^2 m_2^2 m_3^2] dV, \quad (3)$$

where K_1 and K_2 are the anisotropy constants. The magnetostatic energy F_{ms} can be written as,

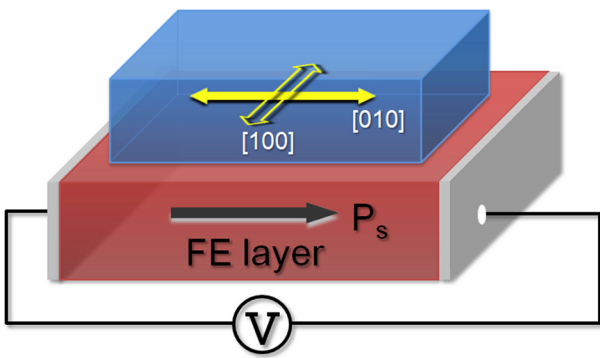


FIG. 1. (Color online) Schematic of a bilayered magnetic/ferroelectric (FE) heterostructure. By applying an appropriate transverse electric field to the bottom FE layer, the domains and/or magnetization in the top magnetic thin film can be switched back and forth between the two principle in-plane crystal axes, i.e., the [100] ($\bar{1}00$) and the [010] ($0\bar{1}0$) directions, respectively. The arrows indicate the magnetization (polarization) in the magnetic (FE) layer.

$$F_{ms} = -\frac{1}{2} \mu_0 M_s \int \mathbf{H}_d \cdot \mathbf{m} dV, \quad (4)$$

where \mathbf{H}_d denotes the stray field arising from the long-range magnetization interaction in the system, given as $\mathbf{H}_d(\bar{\mathbf{M}}) = N\bar{\mathbf{M}}$ ($\bar{\mathbf{M}}$ being the average magnetization field). To simulate magnetization evolution in a sample with specific geometric size, a finite-size magnetostatic boundary condition is used herein, with the demagnetization matrix N computed numerically.²⁷ The exchange energy is determined solely by the special variation of the magnetization orientation and can be formulated as,

$$F_{ex} = A \int (m_{1,1}^2 + m_{1,2}^2 + m_{1,3}^2 + m_{2,1}^2 + m_{2,2}^2 + m_{2,3}^2 + m_{3,1}^2 + m_{3,2}^2 + m_{3,3}^2) dV. \quad (5)$$

Here A is the exchange stiffness constant. $m_{i,j}$ ($i, j = 1, 2, 3$) = $\partial m_i / \partial x_j$, where x_j is the j th component of position vector in the Cartesian coordinates.

The elastic energy F_{elas} can be written as,

$$F_{elas} = \frac{1}{2} \int c_{ijkl} e_{ij} e_{kl} dV = \frac{1}{2} \int c_{ijkl} (\varepsilon_{ij} - \varepsilon_{ij}^0) (\varepsilon_{kl} - \varepsilon_{kl}^0) dV, \quad (6)$$

where e_{ij} is elastic strain, c_{ijkl} the elastic stiffness tensor, and ε_{ij} the total strain that can be represented as the sum of homogenous and heterogeneous strains following Khachaturyan's mesoscopic elastic theory,³³ i.e.,

$$\varepsilon_{ij} = \bar{\varepsilon}_{ij} + \eta_{ij}. \quad (7)$$

The heterogeneous strain η_{ij} is defined in such a way so that $\int_V \eta_{ij} dV = 0$, and the homogeneous strain $\bar{\varepsilon}_{ij}$ describes the macroscopic shape change of the magnetic thin film. Assuming a perfect interface allowing a complete elastic strain transfer between the magnetic and FE layers, the homogenous strains $\bar{\varepsilon}_{11}$ and $\bar{\varepsilon}_{22}$ along the two in-plane crystal axes (i.e., the [100] and [010] axes, respectively, see Fig. 1), can be expressed as,^{2,30}

$$\begin{aligned} \bar{\varepsilon}_{11} &= \varepsilon_0 + d_{31} E, \\ \bar{\varepsilon}_{22} &= \varepsilon_0 + d_{33} E, \end{aligned} \quad (8)$$

upon applying a transverse electric field E to the FE layer poled along the [010] axis (see Fig. 1). Here d_{31} and d_{33} are piezoelectric coefficients of the FE layer, and ε_0 is the biaxial residual strain resulting from the lattice and/or thermal mismatch. The in-plane shear deformation as well as all the stress components in the out-of-plane $\langle 001 \rangle$ direction equals zero following a mixed thin-film mechanical boundary condition,²⁵ i.e.,

$$\begin{aligned} \bar{\varepsilon}_{12} &= \bar{\varepsilon}_{21} = 0, \\ \sigma_{13} &= \sigma_{31} = \sigma_{23} = \sigma_{32} = \sigma_{33} = 0. \end{aligned} \quad (9)$$

ε_{ij}^0 represents the stress-free strain describing the stress-free deformation of a cubic ferromagnet associated with the local magnetization change,

$$\varepsilon_{ij}^0 = \begin{cases} \frac{3}{2}\lambda_{100}(m_i m_j - \frac{1}{3})(i = j), \\ \frac{3}{2}\lambda_{111}m_i m_j (i \neq j), \end{cases} \quad (10)$$

where λ_{100} and λ_{111} are the saturation magnetostrictions measured in the crystal directions $\langle 100 \rangle$ and $\langle 111 \rangle$, respectively. With these in mind, the elastic energy F_{elas} [Eq. (6)] can then be calculated by combining Khachaturyan's elastic theory³³ with Stroh's formalism of anisotropic elasticity.³⁴

To obtain a large strain-mediated ME coupling, the FE layer in our model system [see Fig. 1] is chosen to be the $\langle 001 \rangle$ -poled $\text{Pb}(\text{Zn}_{1/3}\text{Nb}_{2/3})\text{O}_3\text{-PbTiO}_3$ (PZN-PT) single crystal with ultrahigh piezoelectric response ($d_{33} \sim 2000$ pm/V and $d_{31} \sim -1000$ pm/V),³⁵ and cobalt ferrite (CoFe_2O_4 , CFO) with strong magnetoelastic coupling and high Curie temperature¹⁴ is considered as the magnetic film. The temporal evolution of the local magnetization and thus the domain structures in the CFO films are obtained by numerically solving the LLG equation using the semi-implicit Fourier spectral method.³⁶ The bilayer system is discretized into a three-dimensional (3D) array of cubic cells, with finite-size boundary conditions applied along the three principle cubic axes, [100], [010], and [001]. By varying the grid size of each unit cell in real space, two CFO films with different sizes, i.e., $64 \times 64 \times 18$ nm and $192 \times 192 \times 18$ nm, are selected to produce the switching process in a single-domain and multi-domain state, respectively.²⁹ Each simulation proceeds for a long enough time to ensure a stabilized magnetization distribution, with a normalized time step $\Delta\tau = 0.02$. The room-temperature ($T = 298$ K) material parameters of CFO films are listed in Ref. 37.

III. ELECTRIC-FIELD-INDUCED MAGNETIC DOMAIN SWITCHING

As the first example, Fig. 2 shows the electric-field-induced magnetic domain switching in a $64 \times 64 \times 18$ nm (001)-oriented CFO film, which presents a single-domain structure.²⁹ The residual strain mainly results from the lattice mismatch between the CFO film and its bottom PZN-PT layer, which is set as -0.5% for illustration. Note that we employ the cubic magnetic free energy formalisms under such moderate strain herein for simplicity, since significant

deviation resulting from symmetry breaking (e.g., from cubic to tetragonal) usually occurs under very large residual strains (typically with a magnitude higher than 1%).⁴⁰ The latter is more common in ultrathin magnetic films, which rule out the possibility of strain relaxation via, say, the interfacial dislocation. In that case, modifications on the formalisms of magnetocrystalline and magnetoelastic anisotropy are required, such as involving an extra surface magnetocrystalline anisotropy term²¹ and/or high-order magnetoelastic coefficients.⁴⁰ The initial magnetization configurations of the CFO film are assumed to be a uniform [010] [Fig. 2(a)] or [100] [Fig. 2(b)] direction, which can be obtained by subjecting the sample to a high external dc magnetic field. As shown, the magnetization vectors rotate abruptly in the film plane from an initial [010] to a new $[-100]$ direction when the applied transverse electric field E exceeds a positive critical value of 4.2 kV/cm [Fig. 2(a)]. Such an abrupt in-plane 90° switching behavior qualitatively agrees with our previous thermodynamic calculations under a single-domain assumption.^{2,30} Switching to the degenerate [100] direction is also possible under various other electric fields. Moreover, the magnetization vectors would always lie in the film plane and keep a single-domain state even under the application of a much higher positive electric field (not shown here), due to the combined action of the negative (compressive) and positive (tensile) pizeostrains along the [100] and [010] crystal axes, respectively. Compared with Fig. 2(a), a similar switching behavior is observed for the CFO film with a uniform [100] magnetization, as shown in Fig. 2(b). Accordingly, a negative transverse electric field higher than -4.2 kV/cm is required to switch the initial [100] magnetic domain to the [010] or degenerate $[0\bar{1}0]$ directions.

Figure 3(a) shows the electric-field-induced in-plane domain rotation in $192 \times 192 \times 18$ nm (001)-oriented CFO films with a uniform [010] initial magnetization. As seen, a positive transverse electric field higher than 4 kV/cm can switch the magnetization to its perpendicular in-plane [100] or $[\bar{1}00]$ directions while little change is observed upon zero or negative electric fields. Typical magnetic domain structures under various electric fields are illustrated in Fig. 3(b). It can be seen that the CFO film keeps its initial [010] single-domain under a negative electric field of -20 kV/cm. On the other hand, an abrupt in-plane switching to [100] direction takes place when the applied transverse electric field reaches

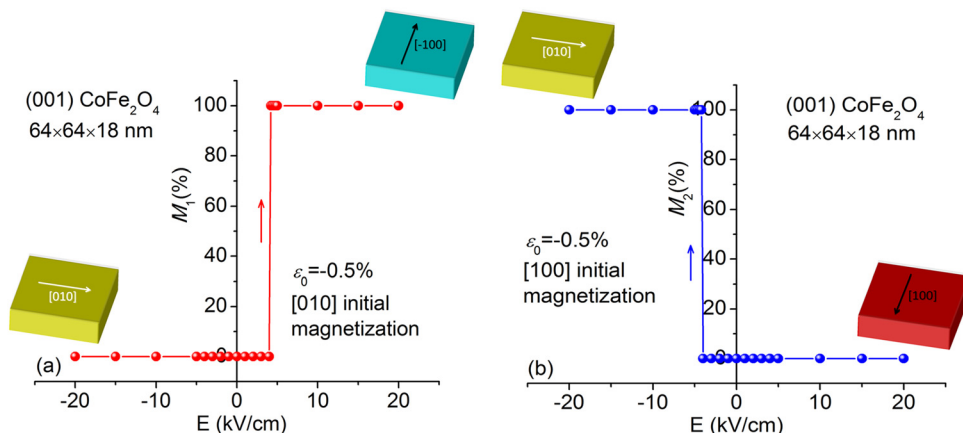


FIG. 2. (Color online) In-plane magnetization switching in a (001)-oriented CoFe_2O_4 (CFO) film of $64 \times 64 \times 18$ nm at $\varepsilon_0 = -0.5\%$, upon application of a transverse electric field E to its adjacent PZN-PT layer. The initial magnetization distributions in the CFO films are assumed to be in (a) the [010] and (b) the [100] directions, respectively. The in-plane magnetization $M_1 = M_{[100]}$ or $M_{[-100]}$, and $M_2 = M_{[010]}$ or $M_{[0\bar{1}0]}$. The insets show the typical domain structures of the CFO films at $E = \pm 20$ kV/cm.

4 kV/cm, resulting in a [100] single-domain structure [see Fig. 3(b)]. Such abrupt switching behavior is somewhat similar to the previous case in single-domain $64 \times 64 \times 18$ nm CFO films. However, the single domain structure is not stable herein, which would change into a stripe-like domain at $E = 5$ kV/cm due to demagnetization along the [100] crystal axis, exhibiting degenerate [100] and $[\bar{1}00]$ domains. Furthermore, as the applied electric field exceeds 10 kV/cm, a checkerboard-like multi-domain structure emerges instead. This is mainly determined by the enhanced in-plane elastic anisotropy energy with increasing electric fields [Eqs. (6) and (8)], which would produce more domains as well as their interfaces, namely, the magnetic domain walls, to minimize the total free energy.^{31,38,39} Moreover, these domain walls gradually become thinner with increasing electric fields [see the narrowing boundaries of the multi-domain structures in Fig. 3(b)].²⁹

In comparison, the electric-field-induced domain switching behavior in $192 \times 192 \times 18$ nm CFO film with a [100] initial magnetization is similar to the case with a [010] initial magnetization, as shown in Fig. 4(a). In this case, the magnetization vectors will keep their initial [100] in-plane direction upon zero or positive transverse electric fields, presenting a [100] single-domain structure [e.g., the domain structure at $E = 20$ kV/cm in Fig. 4(b)]. On the other hand, a negative electric field would rotate the magnetization vectors to the energetically favorable [010] and $[0\bar{1}0]$ directions, resulting in a mixed [010] and $[0\bar{1}0]$ multi-domain structure. Likewise, an abrupt switching feature is observed at $E = -4$ kV/cm

[see Fig. 4(b)]. In comparison to the single domain at $E = 4$ kV/cm for the CFO film with [010] initial magnetization [Fig. 3(b)], a striped-like multi-domain structure is exhibited in this case. This difference can be attributed to a stronger negative piezostain along the [010] axis under negative electric fields, i.e., $d_{33}E < 0$, which dominates the 90° in-plane rotation of the initial [100] domain and further splits the single-domain into multi-domain structure. In contrast, the [010] to [100] domain switching in the previous case is mainly induced by the negative piezostain along the [100] axis upon positive electric fields, i.e., $d_{31}E < 0$, which shows a relatively smaller magnitude and thus may not be sufficient to produce a multi-domain structure. Likewise, the obtained stripe-domain structure would gradually transform into a checkerboard-like domain structure with increasing negative electric fields [see Fig. 4(b)], just as the previous case of CFO films with [010] uniform initial magnetization.

IV. TIME-DEPENDENT ELECTRIC-FIELD-INDUCED MAGNETIC DOMAIN SWITCHING

All the above domain switchings were performed under *static* transverse electric fields applied to the PZN-PT layer, with a uniform [010] or [100] magnetization in the CFO films. To simulate a consecutive domain switching process under *dynamic* electric fields, i.e., electric fields vary with time [e.g., see the square-wave pulse electric field in Fig. 5(a)], the domain structure obtained after the first sequence is used as the initial magnetization distribution in the subsequent simulations.

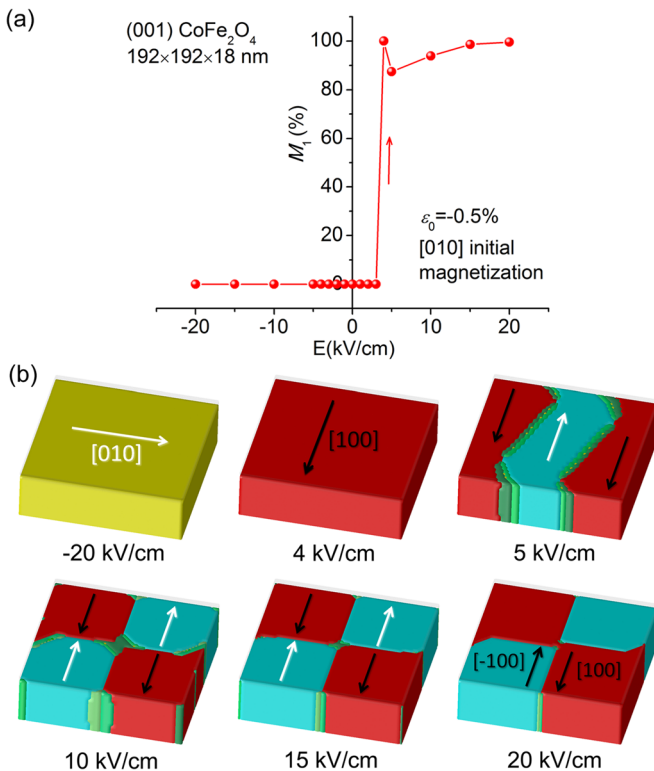


FIG. 3. (Color online) (a) In-plane magnetization, i.e., $M_1 = M_{[100]} + M_{[\bar{1}00]}$, as a function of transverse electric field E in a (001) CoFe_2O_4 (CFO) film of $192 \times 192 \times 18$ nm at $\epsilon_0 = -0.5\%$, with a uniform [010] initial magnetization. (b) Typical magnetic domain structures under various electric fields. The arrows indicate the magnetization directions.

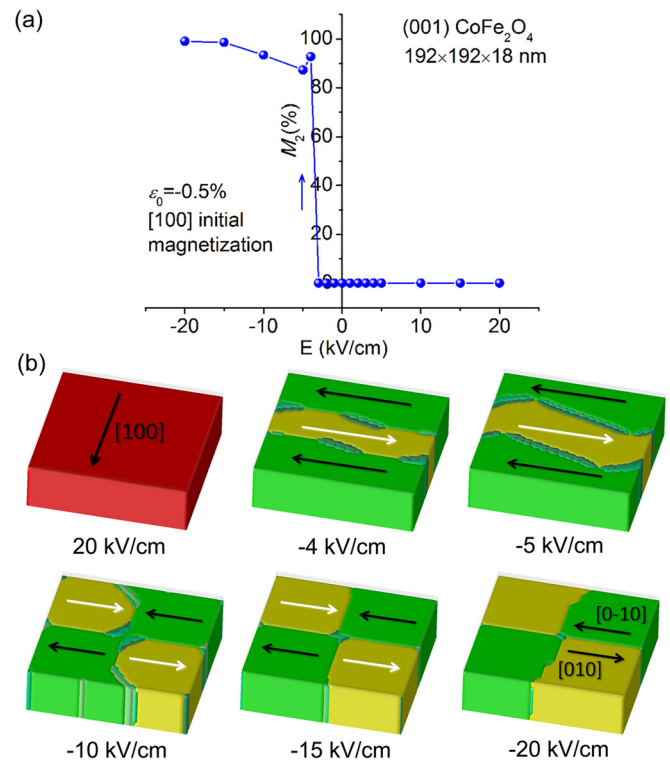


FIG. 4. (Color online) (a) In-plane magnetization, i.e., $M_2 = M_{[010]} + M_{[0\bar{1}0]}$, as a function of transverse electric field E in a (001) CoFe_2O_4 (CFO) film of $192 \times 192 \times 18$ nm at $\epsilon_0 = -0.5\%$, with a uniform [100] initial magnetization. (b) Typical magnetic domain structures under various electric fields. The arrows indicate the magnetization directions.

Figure 5(b) shows the time-dependent electric-field-induced magnetic domain switching feature in single-domain $64 \times 64 \times 18$ nm CFO films. It can be seen that magnetization can be switched back and forth between the initial [010] and $[\bar{1}00]$ directions by a negative and positive transverse electric field of 20 kV/cm, respectively. It is important to point out that the new $[\bar{1}00]$ or [010] single-domain structure obtained after switching can be retained even when the applied electric field falls back to zero [e.g., see the domain structures of sequences 2-3 and 4-5 in Fig. 5(d)].

By comparison, the multi-domain $192 \times 192 \times 18$ nm CFO films present a more complicated time-dependent domain switching feature, as indicated in Fig. 5(c). As shown, the initial [100] single-domain structure remains stable under no external electric fields in sequence 1, i.e., $M_2(\text{net}) = M_{[010]} - M_{[0\bar{1}0]} = 100\%$, due to the relatively strong crystal anisotropy of CFO. A subsequent positive electric field of 20 kV/cm could switch the domains to the

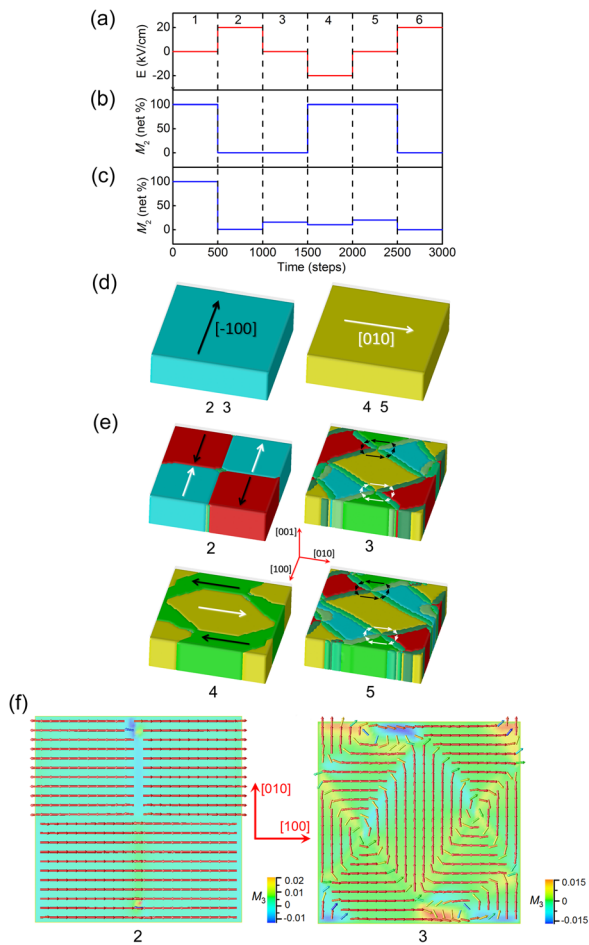


FIG. 5. (Color online) (a) The electric-field-pulse sequence used in simulations. Time-dependent electric-field-induced change of the net magnetization along the [010] crystal axis, i.e., $M_2(\text{net}) = M_{[010]} - M_{[0\bar{1}0]}$, in (001) CoFe_2O_4 (CFO) films of (b) $64 \times 64 \times 18$ nm and (c) $192 \times 192 \times 18$ nm at $\varphi_0 = -0.5\%$. The initial magnetization distribution of the CFO film is assumed to be a uniform [010] magnetization. Corresponding magnetic domain structures in different electric field sequences of the (d) $64 \times 64 \times 18$ nm and (e) $192 \times 192 \times 18$ nm CFO films. The arrows indicate the magnetization directions. (f) Vector plots of the local magnetizations (in top view) of the multi-domain $192 \times 192 \times 18$ nm CFO films in sequences 2 and 3, respectively. A weak out-of-plane magnetization M_3 is exhibited (see the color bar) in these in-plane magnetic domain structures.

degenerate [100] and $[\bar{1}00]$ directions, resulting in a checkerboard-like magnetic domain structure in sequence 2 [see Fig. 5(e)]. In contrast with the single-domain case shown in Figs. 5(b) and 5(d), an in-plane mosaic-like magnetic domain structure emerges when the applied electric fields are removed in sequence 3, leading to a magnetic flux-closure structure [see the arrow circles in the domain structure of sequence 3 in Fig. 5(e)] driven by the demagnetization and the exchange field. To provide more details about such a structure transition, corresponding vector plots of the domain structures of sequences 2 and 3 are illustrated in Fig. 5(f). As shown, typical “head to head” and “tail to tail” domain wall structures in magnetic thin films⁴¹ are exhibited in the checkerboard-like domain structure of sequence 2, under the action of high external electric fields. However, to minimize the demagnetization energy, a 180° Néel-type and 90° in-plane domain wall structure³⁹ are present when electric fields fall back to zero, producing the magnetic flux-closure structure in sequence 3. Furthermore, a negative electric field would switch it into a similar checkerboard-like domain structure in sequence 4, also with the degenerate [010] and $[0\bar{1}0]$ magnetizations. Note that a relatively small net magnetization along the [010] axis is exhibited in this case, i.e., $M_2(\text{net}) = 10.48\%$, only about 10% of the single-domain magnetization value with uniform [010] magnetization in sequence 1. Similar domain switching features take place in the subsequent electric-field sequences of 5 and 6.

In summary, two stable uniform magnetizations of [010] and $[\bar{1}00]$ can be obtained in single-domain $64 \times 64 \times 18$ nm CFO films after applying a negative and positive electric field of 20 kV/cm. This is attributed to the energy barrier provided by the strong magnetocrystalline anisotropy of CFO and can potentially be utilized to develop *nonvolatile* strain-mediated magnetoelectric random access memories (ME-RAMs).³⁰ In multi-domain $192 \times 192 \times 18$ nm CFO films, however, the magnetization configuration can neither be retained after electrical switching nor be rotated back to the initial state upon applying a reverse electric field, governed by the demagnetization and exchange field. Specifically, the latter would become weaker in a larger magnetic thin film system, thus can no longer *lock* the magnetic vectors together to form a single-domain structure. However, this problem can be reduced by the uniaxial exchange coupling interaction between the free layer (i.e., the magnetization vectors are free to rotate) and reference layer (magnetically pinned) in terms of practical ME-RAM device designs.³⁰ Nevertheless, magnetic thin films with a smaller geometric size are in principle more promising for use as the free layers of such ME-RAMs, due to their ease of obtaining bistable magnetization states as discussed above as well as for high-density magnetic storage applications.

V. CONCLUSIONS

In conclusion, electric-field-induced in-plane magnetic domain switching in magnetic/FE layered heterostructures has been studied using phase-field simulations. To achieve a strong strain-mediated converse ME coupling, CFO and PZN-PT with high magnetoelastic coupling and piezoelectric

response are considered as the magnetic and FE layers, respectively. By applying an appropriate transverse electric field to the FE layer, the magnetic domains of the top magnetic films can be switched back and forth between the two principle in-plane crystal axes, i.e., the $[010]/[0\bar{1}0]$ and $[100]/[1\bar{0}0]$ directions. Specifically, a positive electric field would align the magnetic domains along the energetically degenerate $[100]$ and $[1\bar{0}0]$ directions while a negative electric field favors the $[010]$ and $[0\bar{1}0]$ directions. Typical magnetic domain structures of the CFO films under various electric fields are presented.

In $64 \times 64 \times 18$ nm (001)-oriented CFO films, a single-domain structure is exhibited due to the relatively small geometric size,²⁹ and symmetric domain switching behaviors have been observed for the films with uniform $[010]$ and $[100]$ initial magnetization distributions, respectively. The multi-domain $192 \times 192 \times 18$ nm CFO films show a slightly asymmetric switching behavior due to the anisotropic piezostains along the two principal in-plane crystal axes.

Furthermore, the domain switching features under *dynamic* electric fields, i.e., time-dependent electric-field-induced magnetic domain switching, have also been investigated. The results show that bistable uniform magnetization states can be obtained in single-domain $64 \times 64 \times 18$ nm CFO films after applying a negative or positive electric field. In contrast, the magnetization configuration in multi-domain $192 \times 192 \times 18$ nm CFO films can neither be kept stable after electrical switching nor be switched back to the initial state upon reverse electric fields, due to the co-mediation of the demagnetization and exchange field. Such electric-field-induced in-plane magnetic domain switching has potential applications in novel *nonvolatile* strain-mediated ME-RAM devices.³⁰

ACKNOWLEDGMENTS

This work was supported by the National Science Foundation (NSF) under grant number DMR-1006541. The computer simulations were carried out on the LION and Cyberstar clusters at the Pennsylvania State University supported in part by NSF Major Research Instrumentation Program through grant OCI-0821527 and in part by the Materials Simulation Center and the Graduated Education and Research Services at the Pennsylvania State University. This work was also financially supported by the NSF of China (Grant Nos. 50832003 and 50921061), the National Basic Research Program of China (Grant No. 2009CB623303), and in part by the China Scholarship Council.

¹C. W. Nan, M. I. Bichurin, S. X. Dong, D. Viehland, and G. Srinivasan, *J. Appl. Phys.* **103**, 031101 (2008); J. Ma, J.-M. Hu, Z. Li, and C. W. Nan, *Adv. Mater.* **23**, 1062 (2011).

²J.-M. Hu and C. W. Nan, *Phys. Rev. B* **80**, 224416 (2009).

³W. Kleemann, *Physics* **2**, 105 (2009).

⁴H. Ohno, *Nature Mater.* **9**, 952 (2010).

⁵C. Binek and B. Doudin, *J. Phys.: Condens. Mat.* **17**, L39 (2005).

⁶M. Bibes and A. Barthelemy, *Nature Mater.* **7**, 425 (2008).

⁷D. Chiba, M. Sawicki, Y. Nishitani, Y. Nakatani, F. Matsukura, and H. Ohno, *Nature* **455**, 515 (2008).

⁸M. Weisheit, S. Fähler, A. Marty, Y. Souche, C. Poinsignon, and D. Givord, *Science* **315**, 349 (2007).

⁹T. Maruyama, Y. Shiota, T. Nozaki, K. Ohta, N. Toda, M. Mizuguchi, A. A. Tulapurkar, T. Shinjo, M. Shiraishi, S. Mizukami, Y. Ando, and Y. Suzuki, *Nature Nanotechnol.* **4**, 158 (2009).

¹⁰C. A. F. Vaz, J. Hoffman, C. H. Ahn, and R. Ramesh, *Adv. Mater.* **22**, 2900 (2010).

¹¹W. Eerenstein, M. Wiora, J. L. Prieto, J. F. Scott, and N. D. Mathur, *Nature Mater.* **6**, 348 (2007).

¹²S. Sahoo, S. Polisetty, C.-G. Duan, S. S. Jaswal, E. Y. Tsymlal, and C. Binek, *Phys. Rev. B* **76**, 092108 (2007).

¹³C. Thiele, K. Dorr, O. Bilani, J. Rodel, and L. Schultz, *Phys. Rev. B* **75**, 054408 (2007).

¹⁴J. Yang, Y. G. Zhao, H. F. Tian, L. B. Luo, H. Y. Zhang, Y. J. He, and H. S. Luo, *Appl. Phys. Lett.* **94**, 212504 (2009).

¹⁵S. Geprags, A. Brandlmaier, M. Opel, R. Gross, and S. T. B. Goennenwein, *Appl. Phys. Lett.* **96**, 142509 (2010).

¹⁶P. Borisov, A. Hochstrat, X. Chen, W. Kleemann, and C. Binek, *Phys. Rev. Lett.* **94**, 117203 (2005).

¹⁷Y. H. Chu, L. W. Martin, M. B. Holcomb, M. Gajek, S. J. Han, Q. He, N. Balke, C. H. Yang, D. Lee, W. Hu, Q. Zhan, P. L. Yang, A. Fraile-Rodriguez, A. Scholl, S. X. Wang, and R. Ramesh, *Nature Mater.* **7**, 478 (2008).

¹⁸H. Béa, M. Bibes, F. Ott, B. Dupé, X. H. Zhu, S. Petit, S. Fusil, C. Deranlot, K. Bouzehouane, and A. Barthélémy, *Phys. Rev. Lett.* **100**, 017204 (2008).

¹⁹H. J. A. Molegraaf, J. Hoffman, C. A. F. Vaz, S. Gariglio, D. van der Marel, C. H. Ahn, and J. M. Triscone, *Adv. Mater.* **21**, 3470 (2009).

²⁰C. A. F. Vaz, J. Hoffman, Y. Segal, J. W. Reiner, R. D. Grober, Z. Zhang, C. H. Ahn, and F. J. Walker, *Phys. Rev. Lett.* **104**, 127202 (2010).

²¹J.-M. Hu, C. W. Nan, and L. Q. Chen, *Phys. Rev. B* **83**, 134408 (2011).

²²J. van Suchtelen, *Philips Res. Rep.* **27**, 28 (1972).

²³C. G. Zhong, X. M. Ji, Y. L. Zhao, P. X. Zhou, H. X. Cao, and Z. C. Dong, *J. Appl. Phys.* **108**, 084901 (2010).

²⁴L. Q. Chen, *Annu. Rev. Mater. Res.* **32**, 113 (2002).

²⁵L. Q. Chen, *J. Am. Ceram. Soc.*, **91**, 1835 (2008).

²⁶G. Sheng, J. X. Zhang, Y. L. Li, S. Choudhury, Q. X. Jia, Z. K. Liu, and L. Q. Chen, *Appl. Phys. Lett.* **93**, 232904 (2008).

²⁷J. X. Zhang and L. Q. Chen, *Acta Mater.* **53**, 2845 (2005).

²⁸J. X. Zhang, Y. L. Li, D. G. Schlom, L. Q. Chen, F. Zavaliche, R. Ramesh, and Q. X. Jia, *Appl. Phys. Lett.* **90**, 052909 (2007).

²⁹J.-M. Hu, G. Sheng, J. X. Zhang, C. W. Nan, and L. Q. Chen, *Appl. Phys. Lett.* **98**, 112505 (2011).

³⁰J.-M. Hu, Z. Li, J. Wang, and C. W. Nan, *J. Appl. Phys.* **107**, 093912 (2010).

³¹J.-M. Hu, Z. Li, J. Wang, J. Ma, Y. H. Lin, and C. W. Nan, *J. Appl. Phys.* **108**, 043909 (2010).

³²J.-M. Hu, Z. Li, Y. H. Lin, and C. W. Nan, *Phys. Status Solidi RRL* **4**, 106 (2010).

³³A. G. Khachatryan, *Theory of Structural Transformation in Solids* (Wiley, New York, 1983).

³⁴A. N. Stroh, *J. Math. Phys.* **41**, 77 (1962).

³⁵J. Yin and W. Cao, *J. Appl. Phys.* **92**, 444 (2002).

³⁶L. Q. Chen and J. Shen, *Comput. Phys. Commun.* **108**, 147 (1998).

³⁷For CoFe_2O_4 (SI units) at $T=298$ K, $K_1=2 \times 10^5$, $K_2=0$ (Ref. 38); $c_{11}=2.86 \times 10^{11}$, $c_{12}=1.73 \times 10^{11}$, $c_{44}=0.97 \times 10^{11}$, $M_s=3.5 \times 10^5$, $\lambda_{100}=-590 \times 10^{-6}$, $\lambda_{111}=120 \times 10^{-6}$ (Ref. 2); $A=7 \times 10^{-12}$ (Ref. 28).

³⁸B. D. Cullity and C. D. Graham, *Introduction to Magnetic Materials* (2nd ed.) (Wiley, Hoboken, New Jersey, 2009), pp. 227.

³⁹C. Kittel, *Rev. Mod. Phys.* **21**, 541 (1949).

⁴⁰R. C. O'Handley, O. S. Song, and C. A. Ballentine, *J. Appl. Phys.* **74**, 6302 (1993).

⁴¹A. Hubert and R. Schäfer, *Magnetic Domains—The Analysis of Magnetic Microstructures* (Springer-Verlag, Berlin, 2000).